

# Characterising daytime atmospheric conditions on La Palma

Matthew J. Townson<sup>1</sup>, Aglaé Kellerer<sup>2</sup>, James Osborn<sup>1</sup>, Timothy Butterley<sup>1</sup>, Timothy Morris<sup>1</sup>, Richard W. Wilson<sup>1</sup>

<sup>1</sup> Department of Physics, Durham University, South Road, DH1 3LE, UK

<sup>2</sup> Cavendish Laboratory, University of Cambridge, JJ Thomson Avenue, Cambridge CB30HE, UK

E-mail: [matthew.townson@durham.ac.uk](mailto:matthew.townson@durham.ac.uk)

**Abstract.** Day-time turbulence profiles are important for the next generation of Solar Telescopes, which will be equipped with multi conjugate adaptive optics systems. We measured daytime turbulence profiles above La Palma from 17th to 19th September 2013 using a wide-field wave-front sensor. The measured profiles are consistent with previous measurements and suggest that the majority of the turbulence is located close to the ground. Our method does not yet permit precise measurements of high altitude turbulence due to limited instrument and analysis sensitivity.

## 1. Introduction

The next generation of Solar Telescopes, like the Daniel K. Inoue Solar Telescope (DKIST)[1] and the European Solar Telescope (EST)[2] will be equipped with multi-conjugate adaptive optics (MCAO). The optimal operation of these systems requires a precise knowledge of the atmospheric profiles at the telescope site, as well as the integrated seeing[3]. The profiles will influence the design of the MCAO systems: the deformable mirror (DM)s should be optically conjugated to the altitudes of the strongest turbulent layers in the atmosphere.

There is currently little information about the distribution of turbulence in the day-time atmosphere, most information has been extrapolated from night-time conditions, or from surface layer profiles[4].

We present here results from data gathered on La Palma from 17th to 19th September 2013 with the Swedish Solar Telescope (SST)[5] using an S-DIMM+[6], i.e. a wide-field wave-front sensor (WF-WFS). The WF-WFS data was reduced using a SLODAR style analysis[7] to generate turbulence profiles. The location of the instrument is especially relevant as the EST will be situated on Canary Islands[8], and will be equipped with an MCAO system to attain diffraction limited resolution over a  $(2 \times 2)$ arcmin<sup>2</sup> field of view.

## 2. Wide-Field Wave-Front Sensor

The WF-WFS used is similar to the S-DIMM+ previously installed at the SST[6]. The optical components remained unchanged, however the camera was replaced with a larger CMOS chip from Teledyne Dalsa. The camera was run at 100Hz, reading a single row of sub-apertures across



the center of the pupil, as shown in fig 1. Typical data packets span 1 minute to ensure proper sampling of the atmospheric turbulence.

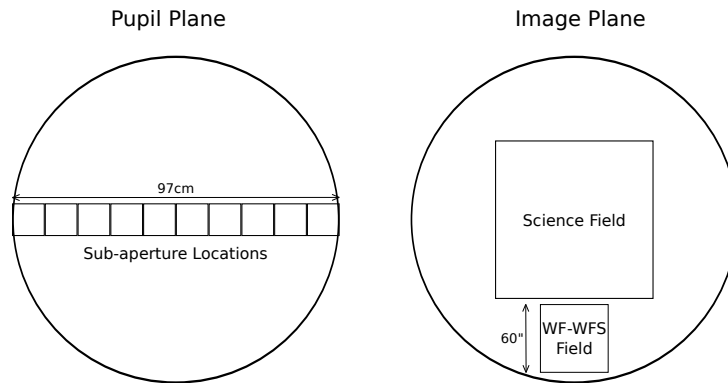


**Figure 1.** The left panel shows the layout of the sub-apertures across the pupil. This gives the maximal number of sub-aperture baselines in one dimension, but also keeps a small footprint on the detector, allowing for faster readout and reduced data sizes. The right panel shows the image plane of the SST: a field stop relays the science field, while a small pick-off relays the the WF-WFS field.

The WF-WFS measures local wave-front gradients as a function of field direction and pupil position. Small regions of the field, that cover a few solar granules, are cross-correlated to obtain the wavefront gradients[9]. The wave-front tilts induced by the turbulence change the position of the granulation on the camera. This displacement is then measured and converted into a local wave-front gradient. The wave-front gradients for different on-sky directions and pupil positions are used to tomographically reconstruct atmospheric profiles via the SLODAR technique[7], as illustrated in fig 2.

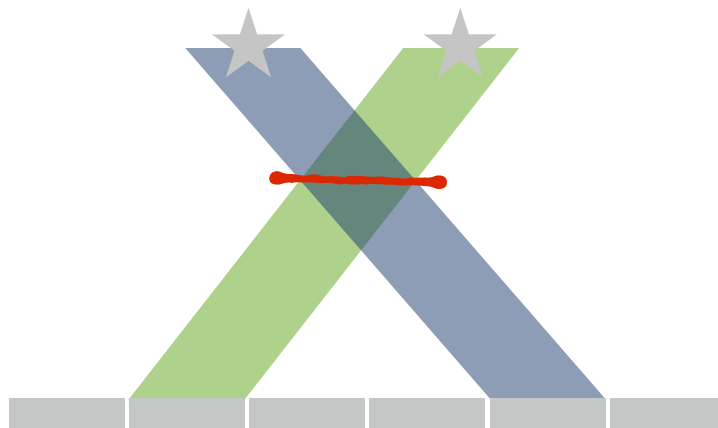


**Figure 2.** Two regions observed by two different sub-apertures. The correlation between the motion of the two sources behind their respective sub-apertures informs about the turbulence over the red surface. The strength of the correlation estimates the strength of the turbulence in that region where the two lines of sight overlap. A full turbulence profile is deduced from measurements behind several sub-apertures and along different field directions.

The cross-correlation of the solar granules is only successful if the seeing is below around  $2''$ :

for larger seeing values the contrast of the granules is too poor to ensure a proper wavefront gradient estimate. There are thus times when the WF-WFS cannot track the solar granulation, and no turbulence profiles can be measured. Typically the seeing deteriorates throughout the day, so in most cases there is a cut-off time after which it is not possible to measure the atmospheric profile due to the deterioration of the seeing. A typical frame from the WF-WFS is shown in fig 3: on this image it is indeed possible to see the solar granulation in the sub-apertures. We measure local wavefront gradients over  $7 \times 8$  small  $6'' \times 6''$  fields that are regularly distributed over the  $53'' \times 60''$  sensor field.

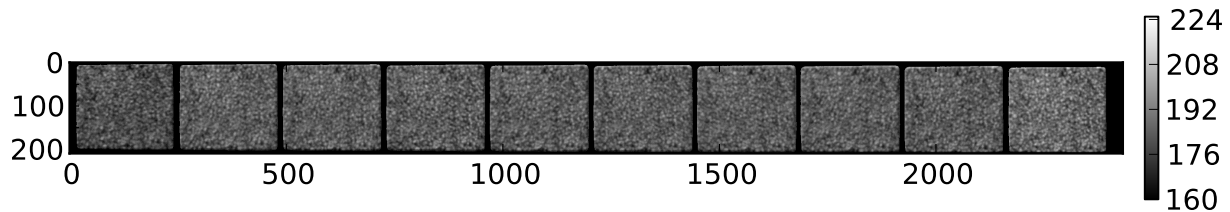


**Figure 3.** A raw frame from the WF-WFS. The ten sub-apertures across the pupil of the SST image the same region of the solar surface. A 610nm filter was used in all observations to optimize the contrast of the solar granulation. The granules are tracked to estimate local wave-front gradients as a function of field direction and sub-aperture. Each sub-aperture images a large field, so many different field directions can be used to estimate the atmospheric profile.

The estimates of the local wavefront gradients are affected by several sources of noise, most importantly tracking errors and wind shake on the telescope. Both shift the solar image uniformly in the focal plane, this shift is identical on all sub-apertures. To remove these effects we subtract the global tip/tilt from every frame, for all field directions. This also removes some signal from the layers of turbulence in the atmosphere: the SLODAR reduction takes this into account by appropriately scaling the global tip/tilt term in the response functions[10].

The resolution of the WF-WFS profiles is not as high as might be expected from the large number of baselines and field directions available. This is because our target is extended: the effective diameter of the sub-apertures therefore increases with altitude. This effect of increasing the size of the sub-apertures decreases the size of the local gradients across the sub-aperture and increases the overlap of the sub-apertures. The final profiles have 10 resolution elements, up to 20km in altitude.

### 3. Results

The profiles taken from the WF-WFS are shown in the left column of fig 4, where the plots run vertically from the 17th - 19th September 2013. The right column of fig 4 shows the average profile on each day.

The profiles all show a similar structure, with most of the power at the ground and some turbulence up to 5km. The lack of detected turbulence above this altitude is likely due to the extended nature of the source. The effective size of the sub-apertures increases with altitude, this not only reduces the resolution of the WF-WFS but also decreases the strength of the correlation signal for turbulence at high altitudes. This makes the profile reconstruction extremely insensitive to high altitude turbulence: the signal from these layers is typically below the noise level. This effect can be mitigated by estimating the wavefront gradients over smaller fields, but then the quality of the correlation - *i.e.* the precision of the gradient estimates - decreases. So although it is in principle possible to sense turbulent layers up to 20km, in practice the strength of high altitude signals is greatly reduced and turbulence at higher altitudes can thus barely be distinguished from noise.

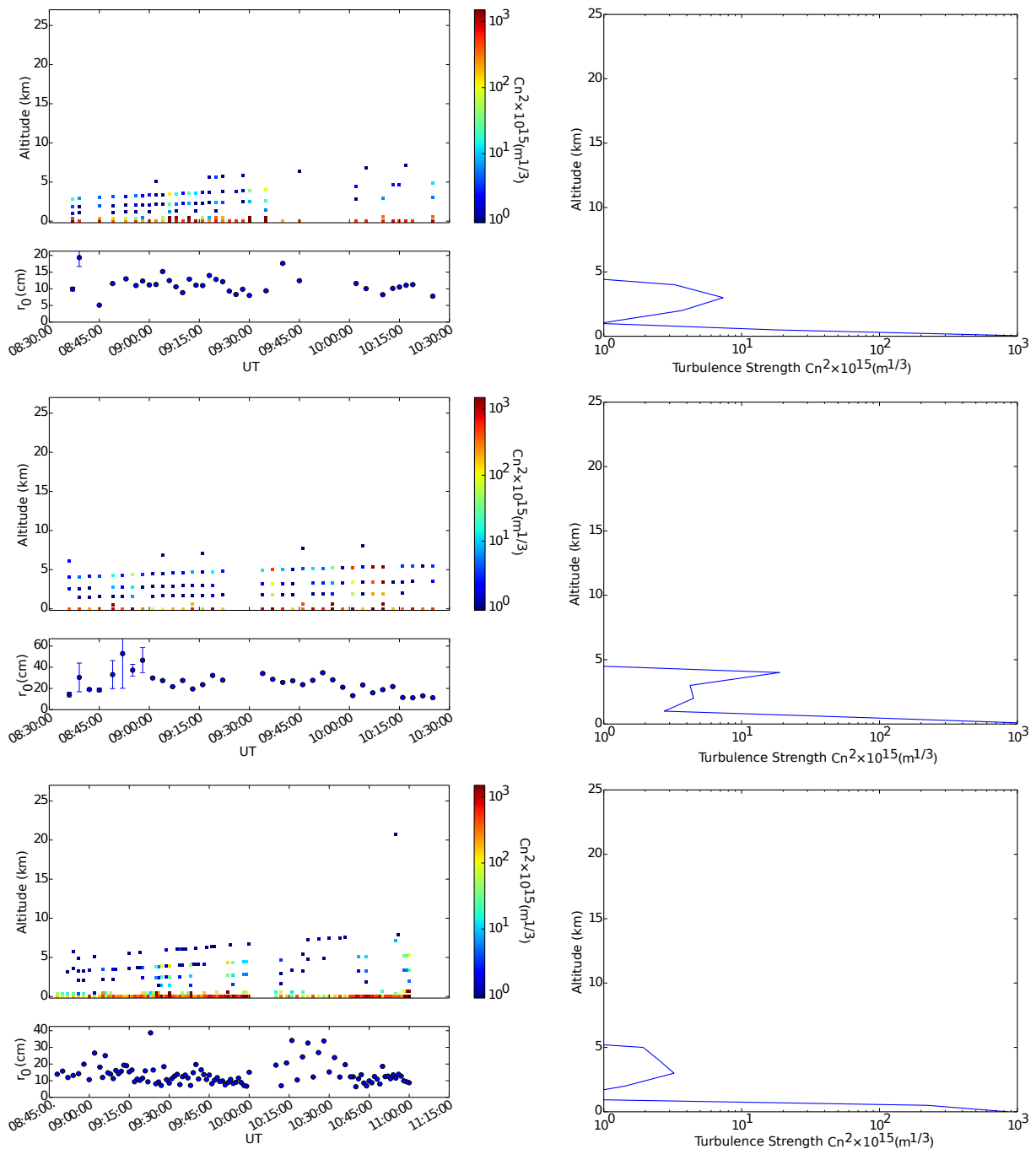


**Figure 4.** The profiles shown in the left column from top to bottom represent the 17th, 18th and 19th September 2013 respectively. The profiles shown on the right show the average turbulence profiles for each day. The profiles all show a strong ground layer, and an extended region of turbulence which peaks in strength around 2.5 to 5km. The estimates of integrated seeing with each of the profiles is shown underneath the profiles.

The average profiles in fig 4 give a clearer impression of the general structure of the turbulence, although all information about the temporal variability of the atmosphere is lost. The average

profiles for each of the days show similar features, with the vast majority of the turbulence located at the ground and a weaker feature between 2.5km and 5km.

#### 4. Conclusions and future work

The profiles presented here are consistent with previous measurements of the daytime atmosphere, which suggested that the majority of the turbulence is located at the ground. We detect no turbulence above 5km, even though the turbulence is expected from the jet stream. The WF-WFS is currently extremely insensitive to high altitude turbulence: this turbulence can only be sensed if it has a similar strength to to the ground layer.

We are currently working on the data analysis to improve the sensitivity to high-altitude turbulence. The WF-WFS will be used in 2015, with a plan to eventually automate the data acquisition and obtain profile estimates in real time.

#### References

- [1] Keil S, Rimmele T and Keller C 2003 *Astronomische Nachrichten* **324** 303–304 ISSN 00046337 URL <http://doi.wiley.com/10.1002/asna.200310103>
- [2] Collados M, Bettonvil F, Cavaller L, Ermolli I, Gelly B, Pérez a, Socas-Navarro H, Soltau D and Volkmer R 2010 *Astronomische Nachrichten* **331** 615–619 ISSN 00046337 URL <http://doi.wiley.com/10.1002/asna.201011386>
- [3] Kellerer A, Gorceix N, Marino J, Cao W and Goode P R 2012 *Astronomy and Astrophysics* **542** A2 ISSN 0004-6361 URL <http://www.aanda.org/10.1051/0004-6361/201218844>
- [4] Berkefeld T, Bettonvil F, Collados M, López R, Martín Y, Peñate J, Pérez A, Scharmer G B, Sliepen G, Soltau D, Waldmann T a and van Werkhoven T 2010 *Proc. SPIE* **7733** 77334I–77334I–10 URL <http://proceedings.spiedigitallibrary.org/proceeding.aspx?articleid=750430>
- [5] Scharmer G B, Bjelksjo K, Korhonen T, Lindberg B and Petterson B 2003 *Proc. SPIE* **4853** 341–350
- [6] Scharmer G B and van Werkhoven T I M 2010 *A & A* **513** A25 ISSN 0004-6361 URL <http://www.aanda.org/10.1051/0004-6361/200913791>
- [7] Wilson R W 2002 *Monthly Notices of the Royal Astronomical Society* **337** 103–108 ISSN 00358711 URL <http://doi.wiley.com/10.1046/j.1365-8711.2002.05847.x>
- [8] Berkefeld T, Bettonvil F, Collados M, López R, Martín Y, Peñate J, Pérez A, Scharmer G B, Sliepen G, Soltau D, Waldmann T a and van Werkhoven T 2010 *Proc. SPIE* **7733** 77334I–77334I–10 URL <http://proceedings.spiedigitallibrary.org/proceeding.aspx?articleid=750430>
- [9] Löfdahl M G 2010 *Astronomy & Astrophysics* **524** A90 ISSN 0004-6361 URL <http://www.aanda.org/10.1051/0004-6361/201015331>
- [10] Butterley T, Wilson R W and Sarazin M 2006 *Monthly Notices of the Royal Astronomical Society* **369** 835–845 ISSN 00358711 URL <http://doi.wiley.com/10.1111/j.1365-2966.2006.10337.x>